Available online at www.sciencedirect.com
SCIENCE DIRECT®
Ocean Modelling 6 (2004) 191–219
Ocean Modelling
www.elsevier.com/locate/omodol

A WKB analysis of the surface signature and vertical structure of long extratropical baroclinic Rossby waves over topography

Rémi Tailleux

Laboratoire de Météorologie Dynamique, case courrier 99, 4 Place Jussieu, 75252 Paris Cédex 05, France

Received 24 January 2002; received in revised form 11 December 2002; accepted 20 December 2002

Abstract

WKB theory has been used recently to construct global approximations of purely periodic long extratropical baroclinic Rossby waves in a continuously stratified ocean, with the goal of building a global theoretical framework that can serve to interpret observed features of the waves, such as sea surface height wave activity and anomalous propagation. This study adopts the same approach in the idealized context of an ocean with constant buoyancy frequency N and longitudinally varying Gaussian topography, to gain insight into issues that have received little or no attention so far, namely: (a) the nature of the links between the vertical structure of the wave field and its surface signature, and the extent to which constraints on the interior dynamics can be derived solely from observing the surface; (b) which of the phase/amplitude variations determine the visual impression of westward propagation, addressed by constructing longitude/time plots of the signal in the attempt to mimic more closely the way the satellite SSH data of TOPEX/Poseidon are analyzed; (c) the validity and accuracy of the classical leading order WKB theory, addressed by estimating the residual a posteriori by computing the next-order term of the formal WKB series expansion. To a lesser extent, this also serves to assess the validity of the planetary geostrophic equations used to describe the dynamics of long Rossby waves.

The main results are that: (a) faster propagation is unambiguously related to the surface intensification of the waves, while slower propagation is associated with a vertical structure intermediate between that of the first and second standard baroclinic modes; (b) westward propagation is dominated by the phase variations; (c) the residual is inversely proportional to the frequency (or equivalently the wavelength by dividing by the phase speed), and is found to vary strongly with position. The hilltop is where the residual is the highest, and hence where WKB is the most likely to breakdown, in agreement with recent published predictions of mode conversion theory in a two-layer model setting.

1463-5003/$ - see front matter
doi:10.1016/S1463-5003(02)00065-3

1. Introduction

1.1. Background and physical issues of interest

Over the past decade, satellite altimetry has modified the way we look at the ocean, and posed new theoretical challenges such as how to link the three-dimensional dynamical structure of dynamical processes to their surface signature. Among the physical processes of interest, planetary waves are of particular importance owing to their prominence in the sea surface height signal (Chelton and Schlax, 1996; Polito and Cornillon, 1997) which make them potentially important for decadal climate variability (Gallego and Cessi, 2000; Cessi and Paparella, 2001). Recently, these waves have attracted considerable theoretical attention after Chelton and Schlax (1996) (CS96 hereinafter) found them: (1) to propagate up to two to three times faster than expected from the linear standard theory (e.g., Gill, 1982; Leblond and Mysak, 1978; Dickinson, 1978) at mid- and high-latitudes; (2) to exhibit significant enhanced activity westward of major topographic features, suggesting a potential topographic influence in amplifying incident waves or/and creating new ones. On this basis, CS96 concluded that the linear standard theory should be revisited. This prompted an intensive research effort aimed at developing an improved oceanic Rossby waves theory, for which the consensus is that it should at least include the effects of the background mean circulation and bottom topography, for both significantly alter the wave dynamics (e.g., Killworth et al., 1997; Dewar, 1998; de Szoeke and Chelton, 1999; Liu, 1999; Yang, 2000; Killworth and Blundell, 2001, for the mean flow effect; Killworth and Blundell, 1999; Tailleux and McWilliams, 2000, 2002; Tailleux, 2002a,b, for topographic effects). An attempt at unifying both effects—so far studied independently—within a single framework was recently undertaken by Killworth and Blundell (2002a,b).

So far, the main approach to study the effects of a varying topography and background mean flow on the propagation and energy dynamics of long, extratropical oceanic Rossby waves has been WKB theory. For the most part, the principal questions addressed are related to the issues raised by CS96, which can be formulated as follows: (I) How do the medium variations affect the local zonal phase speed ω/k_x or group velocity $\partial\omega/\partial k_x$? and how do these modified speeds compare with the observed ones? (II) How do the medium variations affect the rays, i.e., the paths followed by the energy? and what are the consequences for the surface amplitude of the waves? In this paper, we seek to extend the scope of the topics that can be addressed by WKB theory by investigating three important issues that have received little or no attention so far:

(a) The first issue is concerned with linking the tridimensional structure of the waves to their surface signature, taking for granted that the surface of the oceans is now much easier to observe than the interior since the advent of satellite altimetry. Other practical motivations stem from data assimilation, where vertical normal modes are often used, and from the potential possibility of using OGCMs to test the new Rossby wave theories;
(b) The second issue is concerned with determining which of the amplitude/phase variations dominate the visual appearance of westward propagation in longitude/time sections of the sea surface height signal. To answer this question, the computation of the phase, which is often neglected in WKB theory, is required in addition to that of the amplitude. Longitude/time sections, also called Hoevmuller diagrams, have been the traditional means by which the SSH

altimeter data have been analyzed to evidence the westward propagation of the Rossby waves. The principal motivation lies in determining which of the zonal phase speed ω/k_x or group velocity $\partial\omega/\partial k_x$ is the most likely to be measured by CS96, as both quantities have been proposed in the literature. This issue and the previous one are the focus of Section 4.

(c) The third issue is concerned with the validity and accuracy of the classical leading order WKB approximation, and to a lesser extent to that of the PG equations utilized to describe the dynamics of long Rossby waves; these topics are further detailed in the next paragraph, and addressed in Section 5.

1.2. Validity issues

The basic requirement for WKB theory to be valid is that there exists a scale separation between the medium of propagation and the waves. Since this is arguably not realized in the actual ocean, the approach therefore imposes de facto a restriction to topographies and circulations whose small scales have been filtered out. In terms of consequences, it is generally felt that this is not really harmful to estimate the leading order effects of the mean circulation on wave propagation, e.g., the non-WKB approach of Sirven and Frankignoul (2000) yields results similar to that obtained by the WKB approach of Liu (1999), but there is less agreement that this is also true for the topography whose small scales may be important (e.g., Samelson, 1992; Bobrovich and Reznik, 1999; Reznik and Tsybaneva, 1999). The potential pitfalls of neglecting the smaller scales of the topography come from that this directly affects the bottom boundary condition of the eigenvalue problem, whose impact on the eigensolutions may be dramatic as shown by Tailleux and McWilliams (2001) and further discussed in Tailleux (2002b). To date, however, there has been no satisfactory treatment of the rough topographic effect whose study was pioneered by Rhines and Bretherton (1973) (e.g., see Vanneste, 2003, for recent references).

Besides matters of relevance to the actual physical system, the second point of concern with WKB theory is: does it a good job at approximating the actual solutions of the governing equations of motion utilized? The classical view is that the accuracy of the WKB approximation is controlled by the WKB parameter ε, which can be defined here by $\varepsilon = k_\lambda L$, where k_λ is the zonal wavenumber of the Rossby wave, and L a typical scale of (zonal) variations of the medium. If ε is small for a physically reasonable L (but whose choice remains usually quite subjective), then we expect WKB theory to be uniformly valid. The truth, however, is that it is never quite possible to guarantee a priori that WKB theory will work uniformly, except perhaps in the particular one-dimensional case (e.g. see Bender and Orszag, 1978, chapter 10). In general, there are least two well-documented cases of WKB breakdown which may occur even though the subjectively defined ε appears to be far smaller than unity, which are caustics and linear resonance, and whose characteristics are detailed below.

- *Caustics:* A caustic is in some sense the nicest case of WKB breakdown, for its detection is made easy by the fact that it corresponds to the crossing of two rays. At such points, energy focusing occurs on a vanishingly small region and this causes the wave amplitude to become infinite, clearly invalidating the WKB solution. In the present context, caustics may arise for baroclinic rays in a continuously stratified ocean in presence of topography (e.g., Killworth and Blundell, 1999) as a result of the latitudinal variations of the topography and/or those

of the eastern boundary conditions for the wavenumbers (see Tailleux, 2002a). Near caustics, the WKB approximation must be cured by a more accurate procedure which classically involves the Airy function (e.g., Lighthill, 1978). Additional work remains to be done, however, to demonstrate whether known available techniques are applicable in the present context. One step in this direction was recently undertaken by Gorman and Yang (2001) in the context of baroclinic rays propagating through a mean flow, but more work is required to fully elucidate the nature of the wave dynamics near the caustics. In this paper, caustics can be excluded by choosing the topography and the relevant eastern boundary conditions to be independent of latitude (Tailleux, 2002a).

- *Linear resonances:* Linear resonance, which in the literature is often referred to as mode conversion, constitutes a more deleterious case of WKB breakdown because it is not associated to any discontinuity in the rays or leading order variations in the amplitude, so that its occurrence may easily go unnoticed if no specific steps are taken to detect it. Physically, mode conversion occurs when the wavenumbers and frequency of two distinct WKB wave modes supported by the system satisfy approximately the same dispersion relation locally. At such points, the modes become linearly coupled and may resonantly exchange energy. In the present context, this type of phenomenon was first pointed out by Hallberg (1997) (H97) in relation with the linear coupling of bottom and surface intensified Rossby waves over topography in a two-layer QG model of the ocean. H97 also provided empirical formula to predict the amount of energy exchanged between the surface and bottom intensified modes using mass conservation arguments. Vanneste (2001) pointed out that H97's results could be interpreted within the framework of mode conversion theory, for which he pointed out the existence of an extensive literature in plasma physics (e.g., Kaufman and Friedland, 1987; Flynn and Littlejohn, 1994). Actually, Grimshaw and Allen (1979) were arguably the first to study the problem in an oceanic context in relation with the study by Allen and Romea (1980), but this work seems to have been overlooked since. Mode conversion theory was given a fresh start in oceanography by Kaufman et al. (1999), followed more recently by Hallberg (2001) and Tailleux and McWilliams (2002) in the context of two-layer long Rossby wave dynamics over topography.

The main consequence of the existence of caustics and linear resonances is that one should not rely excessively on the a priori (and apparent) smallness of the subjectively defined WKB parameter ε, but always check a posteriori for possible occurrences of WKB breakdown. In this study, this is achieved empirically by computing the next-order term in the formal WKB series expansion, which provides an estimate for the residual of the leading order WKB approximation. The analysis of its spatial structure proves particularly interesting, as it reveals the existence of transition regions occurring over well-determined spatial scales which provide an upper bound for the admissible wavelengths above which WKB will inevitably breakdown, as discussed in Section 5.

1.3. Organization of the paper

This paper is organized as follows. Section 2 presents the planetary geostrophic equations used, their energetics, and the particular configuration studied. Section 3 details the way the leading order WKB approximation for the phase, amplitude and wavenumbers are computed, and pro-

vides the formal way to compute corrections at all orders in ε. Section 4 illustrates the two-abovementioned issues of relating the vertical structure of the waves to their observed surface signature, and to analyze westward propagation directly from longitude/time sections of the WKB approximated sea-surface signal. The a posteriori assessment of the accuracy of the leading order WKB approximation is addressed in Section 5. The results are further discussed in Section 6.

2. The model and its energetics

2.1. The planetary geostrophic model

Following Killworth and Blundell (1999) and Tailleux (2002a), we use the rigid-lid planetary geostrophic equations (PGE) to describe the evolution of perturbations to a resting state characterized by a basic stratification $\rho_0(z)$ function of z only, with time scales long compared to a pendulum day, and with spatial scales large compared to the first baroclinic Rossby radius of deformation. In spherical polar coordinates, the PGE are given by

$$-fv + \frac{1}{R\cos\phi}\frac{\partial p}{\partial \lambda} = 0, \tag{2.1}$$

$$fu + \frac{1}{R}\frac{\partial p}{\partial \phi} = 0, \tag{2.2}$$

$$\frac{\partial p}{\partial z} - b = 0, \tag{2.3}$$

$$\frac{1}{R\cos\phi}\left[\frac{\partial u}{\partial \lambda} + \frac{\partial (v\cos\phi)}{\partial \phi}\right] + \frac{\partial w}{\partial z} = 0, \tag{2.4}$$

$$\frac{\partial b}{\partial t} + N^2(z)w = 0, \tag{2.5}$$

where (u, v, w) is the three-dimensional velocity field, p the pressure divided by a reference density ρ_{ref}, b the buoyancy, $f = 2\Omega\sin\phi$ is the local Coriolis frequency, 2Ω twice the Earth's rotation rate, R the Earth's radius, and $N(z)$ the Brunt–Vaisala or buoyancy frequency. Longitude, latitude, and depth measured upward are denoted by λ, ϕ and z respectively. The boundary conditions are

$$w = 0, \quad \text{at} \quad z = 0, \tag{2.6}$$

$$w = -\mathbf{u}\cdot\nabla H, \quad \text{at} \quad z = -H(\lambda,\phi), \tag{2.7}$$

at the top and bottom of the ocean respectively, where $H(\lambda,\phi)$ is the horizontally dependent total ocean depth, and ∇ the horizontal gradient operator.

2.2. The M-equation

As shown by Welander (1959), the rigid-lid PGE can be expressed in terms of a single variable M, related to the variables of the problem by the relations

$$u = -\frac{1}{2\Omega R \sin\phi}\frac{\partial^2 M}{\partial\phi\,\partial z}, \quad v = \frac{1}{2\Omega R \sin\phi\cos\phi}\frac{\partial^2 M}{\partial\lambda\,\partial z},$$
$$w = \frac{1}{2\Omega R^2 \sin^2\phi}\frac{\partial M}{\partial\lambda}, \quad p = \frac{\partial M}{\partial z}, \quad b = \frac{\partial^2 M}{\partial z^2}.$$

These expressions automatically satisfy the geostrophic approximation (2.1) and (2.2), the hydrostatic approximation (2.3), and the continuity equation (2.4). To satisfy the density equation (2.5) and boundary conditions, M must also satisfy the following equations:

$$\frac{\partial^3 M}{\partial\tilde{t}\,\partial\sigma^2} + \frac{\nu^2(\sigma)}{\sin^2\phi}\frac{\partial M}{\partial\lambda} = 0, \tag{2.8}$$

$$\frac{\partial M}{\partial\lambda}(0) = 0, \tag{2.9}$$

$$\frac{\partial M}{\partial\lambda}(-h) = \tan\phi\left(\frac{\partial^2 M}{\partial\phi\,\partial\sigma}(-h)\frac{\partial h}{\partial\lambda} - \frac{\partial^2 M}{\partial\lambda\,\partial\sigma}(-h)\frac{\partial h}{\partial\phi}\right), \tag{2.10}$$

where non-dimensionalization has been carried out using the following dimensionless variables and parameters:

$$\sigma = \frac{z}{H_0}; \quad \nu(\sigma) = \frac{N}{N_0}; \quad \tilde{t} = \frac{N_0^2 H_0^2}{2\Omega R^2}t; \quad h = \frac{H}{H_0}, \tag{2.11}$$

where H_0 is the maximum ocean depth, and $N_0 = N(0)$.

2.3. Energetics

The rigid-lid PGE are energetically consistent and thus admit an energy conservation equation of the form

$$\frac{\partial E_p}{\partial t} + \mathrm{div}\mathscr{F}_p = 0, \tag{2.12}$$

where the energy E_p and energy flux $\mathscr{F}_p$ are given by

$$E_p = \int_{-H}^{0} b(\lambda,\phi,z,t)z\,\mathrm{d}z, \tag{2.13}$$

$$\mathscr{F}_p = -\int_{-H}^{0}\left(p_0(z) + \frac{\rho_0(z)gz}{\rho_{\mathrm{ref}}}\right)\mathbf{u}(\lambda,\phi,z,t)\,\mathrm{d}z, \tag{2.14}$$

$p_0(z)$ being the hydrostatic pressure of the reference state. The energy (2.13) is potential only, since the geostrophic approximation filters out the kinetic part (Colin de Verdière, 1988). Although (2.12) is the standard form of energy conservation, it is inadequate to derive a wave action conservation law (and thus an amplitude equation for the waves), which must be quadratic in the perturbation amplitudes at leading order (e.g., Shepherd, 1990; Shepherd, 1993) whereas both E_p and $\mathscr{F}_p$ are only linear in the perturbations amplitude. That is, rather than the potential energy, we need the available potential energy in the sense of Lorenz (1955). In the present case, a con-

servation equation quadratic in the perturbations amplitude can be easily obtained directly from the M-equation. This is achieved by multiplying (2.8) by $\partial^2 M/\partial\sigma^2$ after division by v^2, and integrating by parts accounting for the boundary conditions (2.9) and (2.10). After some algebra, the following conservation equation is obtained:

$$\frac{\partial \mathscr{E}}{\partial \tilde{t}} + \frac{1}{\cos\phi}\left[\frac{\partial \mathscr{F}_\lambda}{\partial\lambda} + \frac{\partial(\cos\phi \mathscr{F}_\phi)}{\partial\phi}\right] = 0, \tag{2.15}$$

where

$$\mathscr{E} = \frac{1}{2}\int_{-h}^{0} \frac{1}{v^2}\left(\frac{\partial^2 M}{\partial\sigma^2}\right)^2 \mathrm{d}\sigma, \tag{2.16}$$

$$\mathscr{F}_\lambda = \frac{1}{2}\left[\frac{1}{\sin\phi}\left(\frac{\partial M}{\partial\sigma}(-h)\right)^2 \frac{\partial h}{\partial\phi} - \frac{\cos\phi}{\sin^2\phi}\int_{-h}^{0}\left(\frac{\partial M}{\partial\sigma}\right)^2 \mathrm{d}\sigma\right], \tag{2.17}$$

$$\mathscr{F}_\phi = -\frac{1}{2}\frac{1}{\sin\phi\cos\phi}\left(\frac{\partial M}{\partial\sigma}(-h)\right)^2 \frac{\partial h}{\partial\lambda}. \tag{2.18}$$

As far as we are aware, this important conservation law does not seem to have been recorded before. In terms of the original dynamical variables and dimensional units, the energy and energy fluxes take the following form:

$$\mathscr{E} = \frac{1}{2}\int_{-H}^{0} \frac{b^2}{N^2}\,\mathrm{d}z, \tag{2.19}$$

$$\mathscr{F} = -\frac{1}{2}\frac{\beta}{f^2}\int_{-H}^{0} p^2\,\mathrm{d}z\hat{\mathbf{x}} - \frac{1}{2}\frac{p_\mathrm{b}^2}{f}\hat{\mathbf{z}}\times\nabla H, \tag{2.20}$$

where $p_\mathrm{b} = p(-H)$ is the bottom pressure. The flux is purely westward over a flat-bottom, as expected. Note that the energy is quadratic in the perturbations, so that it can be regarded as an Available Potential Energy for the waves in the sense defined by Shepherd (1993). Note also that the energy flux on a f-plane would follow isobaths in the usual Kelvin wave sense, while in a barotropic ocean for which $p = p_\mathrm{b}$, the energy flux would follow the celebrated f/H contours whose importance was demonstrated in Holland (1967).

2.4. Eastern wavemaker example and numerical values

To illustrate our theoretical results, we consider the example of Rossby waves generated by an eastern wavemaker, as done previously in Killworth and Blundell (1999) and Tailleux and McWilliams (2002). We furthermore assume the buoyancy frequency to be constant, i.e., $N = N_0$, and the topography to be a Gaussian ridge varying with λ only,

$$H(\lambda) = H_0 - \delta H \exp\left\{-\frac{1}{2}\left(\frac{\lambda-\lambda_0}{\lambda_\mathrm{T}}\right)^2\right\}. \tag{2.21}$$

As particular numerical values, we use $H_0 = 4500$ m, $\delta H = 1000$ m, $\lambda_0 = 60°$, $\lambda_\mathrm{T} = 9.6°$. The waves are excited at the eastern boundary of longitude $\lambda_\mathrm{E} = 120°$ at the annual period.

3. The formal WKB series expansion

3.1. The WKB problems at all orders

We seek to construct purely periodic global approximate solutions to (2.8)–(2.10). To that end, we assume that particular (complex) solutions can be sought under the following formal asymptotic expansion:

$$M(\lambda,\phi,\sigma,t) = (M_0(\Lambda,\Phi;\sigma) + \varepsilon M_1(\Lambda,\Phi;\sigma) + \cdots)\mathrm{e}^{\mathrm{i}(\Sigma(\Lambda,\Phi)/\varepsilon-\omega t)}, \tag{3.1}$$

where ε is the assumed small WKB parameter, $(\Lambda,\Phi) = \varepsilon(\lambda,\phi)$ are slow horizontal variables, Σ the usual rapidly varying phase function, while M_0, M_1 etc. are vertical shape functions varying slowly in the horizontal. Real solutions can be obtained by adding the conjugate part. Inserting (3.1) into (2.8)–(2.10) and collecting the terms of equal power in ε, yields at leading order the following eigenvalue problem:

$$-\omega\frac{\mathrm{d}^2M_0}{\mathrm{d}\sigma^2} + \frac{v^2k_\lambda}{\sin^2\phi}M_0 = 0, \tag{3.2}$$

$$M_0(0) = 0; \quad M_0(-h) = \mu M_0'(-h), \quad \mu = \tan\phi\left(\frac{k_\phi}{k_\lambda}\frac{\partial h}{\partial\lambda} - \frac{\partial h}{\partial\phi}\right), \tag{3.3}$$

where $k_\lambda = \partial\Sigma/\partial\Lambda$ and $k_\phi = \partial\Sigma/\partial\Phi$ are the locally defined zonal and meridional wavenumbers respectively.

For $n \geqslant 0$, the next-order problems have the following generic form:

$$-\mathrm{i}\omega\frac{\mathrm{d}^2M_{n+1}}{\mathrm{d}\sigma^2} + \frac{v^2\mathrm{i}k_\lambda}{\sin^2\phi}M_{n+1} = -\frac{v^2}{\sin^2\phi}\frac{\partial M_n}{\partial\lambda}, \tag{3.4}$$

$$\mathrm{i}k_\lambda M_{n+1}(0) + \frac{\partial M_n}{\partial\lambda}(0) = 0, \tag{3.5}$$

$$\mathrm{i}k_\lambda\left[M_{n+1}(-h) - \mu M_{n+1}'(-h)\right] = -\frac{\partial M_n}{\partial\lambda}(-h) + \tan\phi\left[\frac{\partial^2M_n}{\partial\phi\,\partial\sigma}(-h)\frac{\partial h}{\partial\lambda} - \frac{\partial^2M_n}{\partial\lambda\,\partial\sigma}(-h)\frac{\partial h}{\partial\phi}\right]. \tag{3.6}$$

Eqs. (3.4) and (3.5) show that the next-order term M_{n+1} will be in phase quadrature with the term M_n. Thus, if M_0 is real, M_1 will be imaginary an so on. Owing to the particular form of the problem, the real and imaginary parts of M_0 are effectively decoupled, which guarantees that there is no induced geometrical phase (also called Berry's phase), i.e., a phase shift induced by change in the amplitude variations (e.g., see Vanneste and Shepherd, 1999). A geometrical phase, however, would be expected to arise if dispersive effects were retained, as in the QG case for instance.

3.2. The leading order problem

The solution of the leading order problem can be written as $M_0 = AF$, where A is a multiplicative constant to be determined, while F is an eigensolution of:

$$\frac{\mathrm{d}^2F}{\mathrm{d}\sigma^2}+\frac{\nu^2}{\gamma^2}F=0, \tag{3.7}$$

$$F(0)=0, \quad F(-h)=\mu\frac{\mathrm{d}F}{\mathrm{d}\sigma}(-h) \tag{3.8}$$

with

$$\gamma^2=-\frac{\omega\sin^2\phi}{k_\lambda}. \tag{3.9}$$

The eigenvalue problem (3.7) and (3.8) only involves the two parameters μ and h. Its solution can therefore be written formally

$$F=F(\sigma;\mu,h), \quad \Gamma=\gamma^2=\Gamma(\mu,h). \tag{3.10}$$

We illustrate the nature of the solution for a constant buoyancy frequency, previously considered by Rhines (1970) and Straub (1994) for instance. The solution depends on whether γ is real or purely imaginary, i.e., depending on whether γ^2 is positive or negative. Specifically, the expressions for F and F' are respectively given by

$$F(\sigma)=\begin{cases} F_0\sin(\sigma/\gamma) & \text{if } \gamma^2>0,\\ F_0\sinh(\sigma/\gamma) & \text{if } \gamma^2<0,\end{cases} \quad F'(\sigma)=\begin{cases} \frac{F_0}{\gamma}\cos(\sigma/\gamma) & \text{if } \gamma^2>0,\\ \frac{F_0}{\gamma}\cosh(\sigma/\gamma) & \text{if } \gamma^2<0,\end{cases} \tag{3.11}$$

where F_0 is a normalization constant. The bottom boundary condition imposes the following constraint on γ:

$$\begin{cases} \tan(h/\gamma)=-\frac{\mu}{\gamma} & \text{if } \gamma^2>0,\\ \tanh(h/\gamma)=-\frac{\mu}{\gamma} & \text{if } \gamma^2<0.\end{cases} \tag{3.12}$$

A condensed representation of the eigenvalues can be obtained if we pose $X=h/\gamma$ and $\alpha=\mu/h$, in which case (3.12) becomes

$$\begin{cases} \tan\alpha+\alpha X=0 & \text{if } \gamma^2>0,\\ \tanh\alpha+\alpha X=0 & \text{if } \gamma^2<0.\end{cases} \tag{3.13}$$

Such a problem admits an infinite number of discrete solutions, which we formally denote by $X_n=S_n(\alpha)$. As a result, we can write $\Gamma=\gamma^2$ under the following form:

$$\Gamma=\gamma^2=\frac{h^2}{S_n^2(\mu/h)}\Rightarrow\frac{h^2}{\Gamma(\mu,h)}=S_n^2(\mu/h). \tag{3.14}$$

Given that h is usually known, the complete knowledge of Γ is obtained from that of S_n^2 as a function of $\mu/h\equiv\alpha$. The resulting dispersion curves are illustrated in Fig. 1. In this paper, we shall mainly be concerned with the behavior along the curve $n=1$ which for $\mu=0$ corresponds to the standard first baroclinic mode. Note, however, that this mode can actually become a second mode for negative values of the parameter μ/h, since then the mode $n=0$, which does not exist for positive value of μ/h, takes over the lead role of first mode there. In the wavemaker experiment considered here, this occurs on the ridge's eastern flank for instance. As a result, slower propagation than standard ensues. It is important to realize, however, that the mode $n=0$, which is

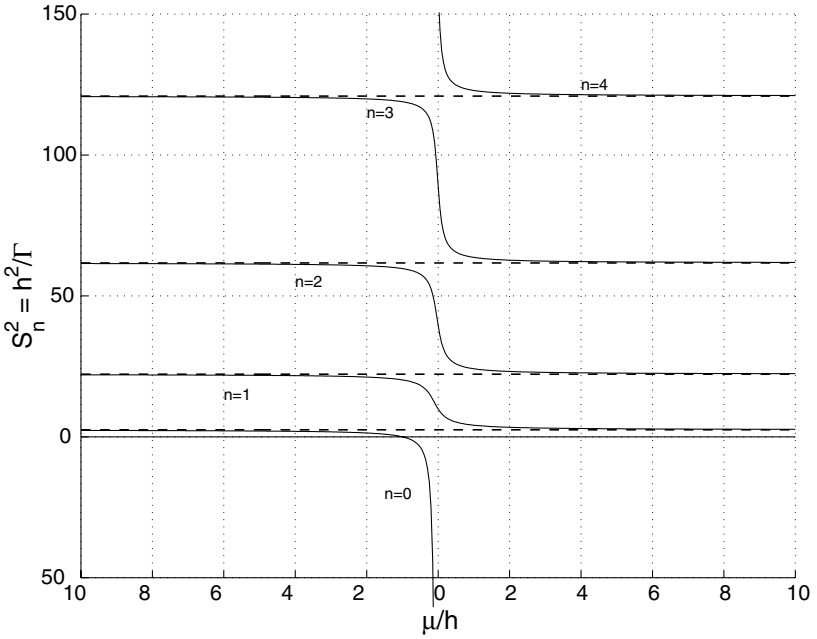

Fig. 1. The dispersion curves $S_n^2(\mu/h) = h^2/\Gamma_n(\mu, h)$ for $n = 0, 1, 2, 3, 4$.

faster than the flat-bottom baroclinic mode, might also be present in the surface signal for negative values of μ. Such a mode cannot be evidenced in the present single-mode WKB theory, but we speculate that it may be present in wind-forced experiments for instance. We believe that the existence of this mode, not discussed in Killworth and Blundell (1999), is potentially important to determine whether topographic effects may significantly contribute to the "too fast" Rossby wave issue (see Tailleux, 2002b, for further discussion).

3.3. Dispersion relation, ray dynamics, and phase determination

With the above notations, (3.9) provides the dispersion relation under the form:

$$\omega = -\frac{k_\lambda}{\sin^2\phi}\Gamma(\mu, h). \tag{3.15}$$

The next step is to provide evolution equations for the wavenumbers along particular directions called rays, which are given by (e.g., Lighthill, 1978):

$$\frac{\mathrm{D}\mathbf{x}}{\mathrm{D}s} = \frac{\partial\omega}{\partial\mathbf{k}} = \mathbf{c}_\mathrm{g}, \quad \frac{\mathrm{D}\mathbf{k}}{\mathrm{D}s} = -\frac{\partial\omega}{\partial\mathbf{x}}, \tag{3.16}$$

where $\mathbf{x} = (\lambda, \phi)$, while $\mathbf{c}_\mathrm{g}$ is the group velocity. By differentiating (3.15) with respect to k_λ and k_ϕ, as shown in Tailleux (2002a), one shows that:

$$c_{\mathrm{g}\lambda} = -\frac{\Gamma^2 K_\mathrm{I}^2}{\sin^2\phi} + \frac{\Gamma^2 K_\mathrm{b}^2}{\sin\phi\cos\phi}\frac{\partial h}{\partial\phi}, \quad c_{\mathrm{g}\phi} = -\frac{\Gamma^2 K_\mathrm{b}^2}{\sin\phi\cos\phi}\frac{\partial h}{\partial\lambda}, \tag{3.17}$$

where

$$K_{\rm I}^2 = \frac{\int_{-h}^{0} F'^2 \,\mathrm{d}\sigma}{\int_{-h}^{0} v^2 F^2 \,\mathrm{d}\sigma}, \quad K_{\rm b}^2 = \frac{F_{\rm b}'^2}{\int_{-h}^{0} v^2 F^2 \,\mathrm{d}\sigma}, \tag{3.18}$$

where $F' = \mathrm{d}F/\mathrm{d}\sigma$ and $F_{\rm b}' = \mathrm{d}F/\mathrm{d}\sigma(-h)$. This result is similar to that obtained by Killworth and Blundell (1999) using different notations. The expressions for $K_{\rm I}^2$, $K_{\rm b}^2$ and other related coefficients are derived in Appendix A for the constant buoyancy case, and illustrated in Fig. 10.

In WKB theory, the phase usually receives less attention than the amplitude. It is nevertheless important in the present context, as it is central to understand the observed propagation features of Rossby waves, as discussed further in the text. There is several ways to compute it. One way consists in deriving an evolution equation of the phase along the rays (e.g., Vanneste and Shepherd, 1999). To that end, we introduce the factor $\mathscr{J} = \mathbf{c}_{\rm g} \cdot \mathbf{k}/\omega$, [1] which allows to rewrite the dispersion relation as $\omega = \mathbf{c}_{\rm g} \cdot \mathbf{k}/\mathscr{J}$, or in terms of the phase function Σ,

$$\left(c_{{\rm g}\lambda} \frac{\partial \Sigma}{\partial \lambda} + c_{{\rm g}\phi} \frac{\partial \Sigma}{\partial \phi} \right) = \mathscr{J} \omega \tag{3.19}$$

which can also be written as a first order ordinary differential along the rays as follows:

$$\frac{\mathrm{D}\Sigma}{\mathrm{D}s} = \mathscr{J}\omega \Longleftrightarrow \frac{\mathrm{D}\Sigma}{\mathrm{D}\lambda} = \frac{\mathscr{J}\omega}{c_{{\rm g}\lambda}}, \tag{3.20}$$

where $\mathrm{D}/\mathrm{D}\lambda = \partial_\lambda + c_{{\rm g}\phi}/c_{{\rm g}\lambda}\partial_\phi$ represents the λ-derivative along the ray. In the present case, it is easy to show that the factor $\mathscr{J}$ simply reduces to unity. This stems from the particular form of the dispersion relation which can be written as $\omega = kG(\theta)$, with $G(\theta) = -\Gamma(\mu, h)\cos\theta/\sin^2\phi$, where (k, θ) is the polar representation of the wavevector, i.e., $k_\lambda = k\cos\theta$ and $k_\phi = k\sin\theta$. This is because $\mu = \tan\phi(\tan\theta\partial_\lambda h - \partial_\phi h)$ only depends on θ. In polar coordinates, the group velocity reads

$$\mathbf{c}_{\rm g} = \nabla_{\mathbf{k}}\omega = \frac{\partial\omega}{\partial k}\hat{\mathbf{u}}_k + \frac{1}{k}\frac{\partial\omega}{\partial\theta}\hat{\mathbf{u}}_\theta = G(\theta)\hat{\mathbf{u}}_k + G'(\theta)\hat{\mathbf{u}}_\theta, \tag{3.21}$$

where $\hat{\mathbf{u}}_k = (\cos\theta, \sin\theta)$ and $\hat{\mathbf{u}}_\theta = (-\sin\theta, \cos\theta)$ are the unit vectors pointing in the direction of $\mathbf{k}$ and rotated by $\pi/2$ respectively. Multiplying (3.21) by $\mathbf{k} = k\hat{\mathbf{u}}_k$ yields immediately $\mathbf{c}_{\rm g} \cdot \mathbf{k} = kG(\theta) = \omega$, hence $\mathscr{J} = \mathbf{c}_{\rm g} \cdot \mathbf{k}/\omega = 1$. [2]

Since $\mathscr{J} = 1$ and ω is constant, the integration of (3.20) yields $\Sigma = \Sigma(s = 0) + \omega s$, which requires an expression for s. While this can be done in general, it appears simpler in the present case

[1] The vector $\mathbf{S} = \mathbf{k}/\omega$ is often called the "slowness" vector in the seismological literature. Such a vector obeys the usual projection rule for vectors, so that $S_n = \mathbf{S} \cdot \mathbf{n}$ defines appropriately the slowness in the direction of unit normal vector $\mathbf{n}$. In this respect, $\mathbf{S}$ behaves better than the "fundamental" phase velocity vector $\mathbf{C}_p = \omega\mathbf{k}/\|\mathbf{k}\|^2$, which does not satisfy the projection rule for vectors (e.g., see Pedlosky, 1987). On the other hand, the inverse of the slowness in the direction $\mathbf{n}$, i.e., the quantity $C_n = (\mathbf{S} \cdot \mathbf{n})^{-1}$ defines the phase speed in the direction $\mathbf{n}$. Thus, one may write $\mathscr{J} = \mathbf{c}_{\rm g} \cdot \mathbf{S}$, and interpret $\|\mathbf{c}_{\rm g}\|/\mathscr{J}$ as the phase speed in the direction of the group velocity.

[2] More generally, one shows that if the dispersion relation is of the form $\omega = k^\alpha G(\theta)$, then $\mathscr{J} = \alpha$. Note that the dispersion relation is of the form $\omega = kG(\theta)$ for all models based on the planetary geostrophic equations (see remark in Killworth and Blundell, 2002a,b). For classical QG Rossby waves on the β-plane, one shows that $\mathscr{J} = (1 - k^2R_{\rm o}^2)/(1 + k^2R_{\rm o}^2) \neq 1$, where $R_{\rm o}$ is the Rossby radius of deformation.

to determine the phase directly from the knowledge of the wavenumbers. Indeed, it is a simple matter to integrate the differential system:

$$k_\lambda = \frac{\partial \Sigma}{\partial \lambda}, \quad k_\phi = \frac{\partial \Sigma}{\partial \phi}, \tag{3.22}$$

provided that k_λ and k_ϕ are known functions of λ and ϕ. In practice, this requires to invert the function $\phi(\lambda, \xi)$ to get $\xi(\lambda, \phi)$, as integration along the rays yields the wavenumbers in the (λ, ξ) coordinates system, rather than in the (λ, ϕ) coordinates system. Here, ξ is a ray index representing the ray launching latitude along the eastern boundary. It turns out that this is easy to do for the present idealized situation. To that end, we first invoke the results of Tailleux (2002a) establishing that the canonical ray equations (3.16) can be reduced down to two ordinary differential equations for $Z = \tan\phi k_\phi/k_\lambda$ and the function $\chi(\lambda, \xi) = \sin\phi(\lambda, \xi)/\sin\xi$. For a topography varying with λ only, the ODEs for Z and χ are given by

$$\frac{\mathrm{D}Z}{\mathrm{D}\lambda} = \frac{2}{\Gamma K_\mathrm{I}^2} + K_\mathrm{r}^2 Z\left[Z\frac{\mathrm{d}^2 h}{\mathrm{d}\lambda^2} + \left(1 + \frac{v_\mathrm{b}^2 Z^2 (\mathrm{d}h/\mathrm{d}\lambda)^2}{\Gamma}\right)\frac{\mathrm{d}h}{\mathrm{d}\lambda}\right], \tag{3.23}$$

$$\frac{\mathrm{D}\ln\chi}{\mathrm{D}\lambda} = K_\mathrm{r}^2 \frac{\mathrm{d}h}{\mathrm{d}\lambda}, \tag{3.24}$$

where $K_\mathrm{r}^2 = K_\mathrm{b}^2/K_\mathrm{I}^2$. The latter coefficient is illustrated as a function of μ in Appendix A. The equation for Z is obtained by combining the evolution equations for k_λ, k_ϕ and ϕ, while that for χ is deduced from that for ϕ (see Tailleux and McWilliams, 2002, for details). The idea underlying this decomposition is that the solution of the eigensystem depends on only one ray-depending parameter, which is $\mu = Zh'(\lambda)$ for a topography varying with longitude only.

We integrate these equations westward with the eastern boundary conditions $Z(\lambda_\mathrm{E}) = \ln\chi(\lambda_\mathrm{E}) = 0$, corresponding respectively to assuming $\Sigma = cst$ along the meridian of longitude $\lambda = \lambda_\mathrm{E}$, and $\phi(\lambda_\mathrm{E}, \xi) = \xi$. We also use $v_\mathrm{b} = v = 1$. For such a case, i.e., the topography varying with λ only and the boundary condition independent of the ray index ξ, Tailleux (2002a) shows that Z and χ are functions of λ only. The longitude of the ray $\phi(\lambda, \xi)$, and the wavenumbers are related to Z and χ by the following relations:

$$\sin\phi = \chi(\lambda)\sin\xi, \tag{3.25}$$

$$k_\lambda = -\frac{\omega\sin^2\phi}{\Gamma(\lambda)} = -\frac{\omega\chi^2(\lambda)}{\Gamma(\lambda)}\sin^2\xi, \tag{3.26}$$

$$k_\phi = \frac{Zk_\lambda}{\tan\phi} = -\frac{\omega\sin\phi\cos\phi Z(\lambda)}{\Gamma(\lambda)}. \tag{3.27}$$

The result for Z, χ and Γ is displayed in Fig. 2. The top panel shows that Z on average decreases westward (thick line). For comparison, the flat-bottom behavior of Z (dashed line) is also plotted. Note that $|Z|$ over a flat-bottom increases westward because the latitudinal variations of f and β are retained, i.e., the speed of long Rossby waves varies with latitude in the PG system. For the classical QG Rossby waves over a β-plane, Z would remain constant, because the speed of long Rossby waves is independent of latitude in this framework. The function χ (middle panel) provides a direct indication of the ray behavior, since $\sin\phi = \chi(\lambda)\sin\xi$. Here the ray is seen to be

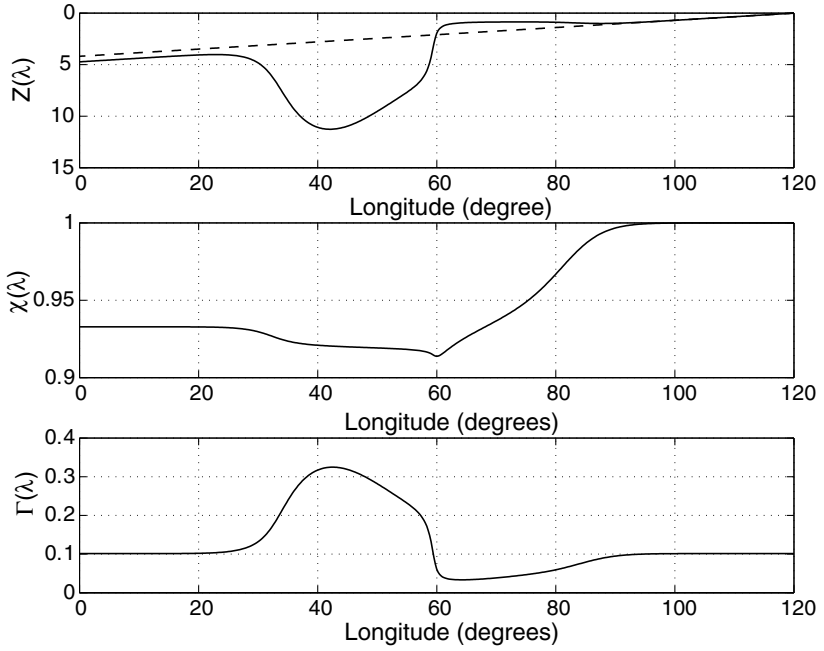

Fig. 2. The function $Z = \tan\phi k_\phi/k_\lambda$ (bottom), $\chi = \sin\phi/\sin\xi$ (middle), and $\Gamma = -\omega\sin^2\phi/k_\lambda$ (bottom) as a function of longitude for the eastern wavemaker experiment using a constant buoyancy frequency, where ξ is the ray index defined at the launching latitude of the ray along the eastern boundary. Physically, Γ represents the zonal phase speed multiplied by $\sin^2\phi$; it is also a measure of the vertical intensification of the flow (see text for details).

deflected southward up to the ridge's top, after what it is slightly deflected northward. We note that χ remains close to unity, which means that the ray departs little from a purely zonal behavior. The function Γ (bottom panel) provides an indication of how the local zonal phase speed $c_{p\lambda}$ evolves along the ray. Here, we see that slower propagation than standard occurs on the eastern flank, while faster propagation than standard is found on the western flank, in agreement with the previous results of Killworth and Blundell (1999); Tailleux and McWilliams (2002) and Tailleux (2002a). The same kind of behavior is also found if a different initial condition for Z is chosen provided that it is negative. However, this behaviour may be reversed if a large enough positive initial condition is chosen for Z, i.e., faster propagation on the eastern flank and slower on the western one, because this reverses the sign μ takes on each flank. The regions of fastest transition, however, are not affected by the initial condition chosen for Z.

Eq. (3.25) yields either $\phi(\lambda,\xi) = \arcsin[\chi(\lambda)\sin\xi]$ or $\xi(\lambda,\phi) = \arcsin[\sin\phi/\chi(\lambda)]$. The expression (3.26) expresses k_λ both in terms of (λ,ϕ) and (λ,ξ). From the first form, integration in λ yields

$$\Sigma(\lambda,\phi) = -\omega\sin^2\phi\int_{\lambda_E}^{\lambda}\frac{\mathrm{d}\lambda'}{\Gamma(\lambda')}. \tag{3.28}$$

This form is similar to that obtained previously by Killworth and Blundell (1999). As an illustration, the function $\Sigma^\star(\lambda) = \Sigma/(\omega\sin^2\phi)$, which depends on λ only, is depicted in Fig. 3. We

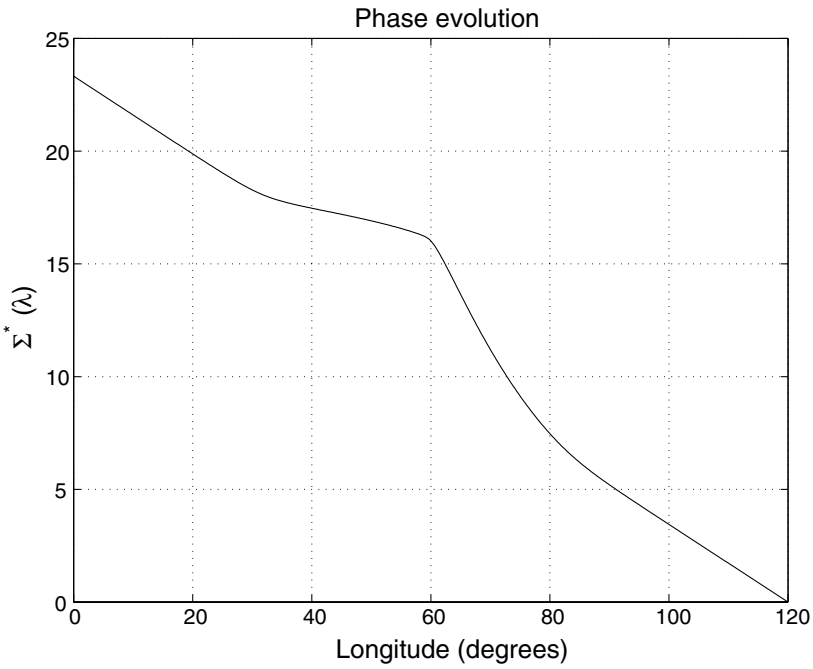

Fig. 3. The normalized phase function $\Sigma^\star(\lambda) = \Sigma/(\omega \sin^2\phi)$ as a function of longitude.

note that the phase evolves in an essentially piecewise linear way. This comes from that Σ, as an integral function of Γ, smoothes out relatively nonlinear variations of Γ (see Fig. 2, bottom).

3.4. Amplitude equations for $|A|$ and $|p_s|$

The evolution equation for the amplitude $|A|$ can be constructed either as a compatibility condition of the next-order problem, or more directly by inserting the leading order approximation $\Re(M) \approx AF\mathrm{e}^{\mathrm{i}(\Sigma/\varepsilon-\omega t)} + \text{c.c.}$ into the energy conservation equation (2.15), and averaging over one period ($\Re$ denotes real part). Choosing the latter method yields

$$\mathscr{E} = \frac{|A|^2}{2}\int_{-h}^{0}\frac{1}{v^2}\left(\frac{\mathrm{d}^2F}{\mathrm{d}\sigma^2}\right)^2\mathrm{d}\sigma = \frac{|A|^2}{2\gamma^4}\int_{-h}^{0}v^2F^2\,\mathrm{d}\sigma = \frac{|A|^2}{2\Gamma^2}\int_{-h}^{0}v^2F^2\,\mathrm{d}\sigma, \tag{3.29}$$

$$\mathscr{F}_\lambda = \frac{|A|^2}{2}\left[\frac{F_\mathrm{b}'^2}{\sin\phi}\frac{\partial h}{\partial\phi} - \frac{\cos\phi}{\sin^2\phi}\int_{-h}^{0}F'^2\,\mathrm{d}\sigma\right], \tag{3.30}$$

$$\mathscr{F}_\phi = -\frac{|A|^2}{2}\frac{F_\mathrm{b}'^2}{\cos\phi\sin\phi}\frac{\partial h}{\partial\lambda}. \tag{3.31}$$

We note that the energy flux components can be written in terms of the group velocity components as follows:

$$\mathscr{F}_\lambda = \cos\phi c_{\mathrm{g}\phi}\mathscr{E}, \quad \mathscr{F}_\phi = c_{\mathrm{g}\lambda}\mathscr{E} \tag{3.32}$$

so that, given that $\mathscr{E}$ is independent of time, yields the following conservation equation:

$$\frac{\partial}{\partial\lambda}\left(c_{g\lambda}\mathscr{B}|A|^2\right)+\frac{\partial}{\partial\phi}\left(c_{g\phi}\mathscr{B}|A|^2\right)=0, \tag{3.33}$$

where

$$\mathscr{B}(\mu,h;\phi)=\frac{\cos\phi}{\Gamma^2}\int_{-h}^{0}v^2F^2\,\mathrm{d}\sigma. \tag{3.34}$$

Eq. (3.33) has the usual form of the ray tube conservation of action of Lighthill (1978), provided that we see $\mathscr{B}|A|^2$ as the relevant action here. Since we are interested in the surface signature of the waves, we also seek to derive a conservation equation for the surface pressure amplitude. To that end, we use the result that at leading order,

$$p_s(\lambda,\phi,t)=\Re\left(\frac{\partial M}{\partial\sigma}(0)\right)\approx AF'(0)\mathrm{e}^{\mathrm{i}(\Sigma-\omega t)}+\text{c.c.} \tag{3.35}$$

If we denote $|\hat{p}_s|=|AF'(0)|$, Eq. (3.33) can be rewritten as follows:

$$\frac{\partial}{\partial\lambda}\left(\cos\phi c_{g\lambda}\frac{|\hat{p}_s|^2}{\Gamma^2K_0^2}\right)+\frac{\partial}{\partial\phi}\left(\cos\phi c_{g\phi}\frac{|\hat{p}_s|^2}{\Gamma^2K_0^2}\right)=0, \tag{3.36}$$

where

$$K_0^2=\frac{F'^2(0)}{\int_{-H}^{0}v^2F^2\,\mathrm{d}\sigma}. \tag{3.37}$$

We simplify (3.36) using the result demonstrated in Tailleux and McWilliams (2002) (Appendix A) that a conservation law of the form $\partial_\lambda(c_{g\lambda}F_\lambda)+\partial_\phi(c_{g\phi}F_\phi)=0$ can be rewritten in the coordinate system (λ,ξ) as $\phi_\xi^{-1}\partial_\lambda(\phi_\xi c_{g\lambda}F_\lambda)=0$, where the derivative in λ is taken along the rays, while $\phi_\xi=\partial\phi/\partial\xi$. Physically, $\phi_\xi\,\mathrm{d}\xi$ represents the infinitesimal spacing between the two rays of index ξ and $\xi+\mathrm{d}\xi$. From (3.17), we have $c_{g\lambda}=-\Gamma^2K_I^2/\sin^2\phi$, since $\partial_\phi h=0$ here. In the end, (3.36) becomes

$$\frac{\partial}{\partial\lambda}\left[\phi_\xi\frac{\cos\phi}{\sin^2\phi}\frac{K_I^2|\hat{p}_s|^2}{K_0^2}\right]=0, \tag{3.38}$$

where the derivative is understood to be taken along the rays, i.e., for fixed ray index ξ. Differentiating (3.25) with respect to ξ yields

$$\cos\phi\phi_\xi=\cos\xi\chi(\lambda)\Rightarrow\phi_\xi=\frac{\cos\xi}{\cos\phi}\chi(\lambda)$$

and the fact that $\sin\phi=\sin\xi\chi(\lambda)$, we arrive at the formula

$$\frac{\cos\xi}{\sin^2\xi}\frac{\partial}{\partial\lambda}\left[\frac{1}{\chi(\lambda)}\frac{K_I^2|\hat{p}_s|^2}{K_0^2}\right]=0 \tag{3.39}$$

because the terms involving ξ are constant along the rays, and thus can be taken out of the derivative. The results of Appendix A yield

$$\frac{K_{\mathrm{I}}^2}{K_0^2} = \frac{h}{2}\frac{1-\alpha+\alpha^2 S_n^2(\alpha)}{1+\alpha^2 S_n^2(\alpha)} \tag{3.40}$$

which thus is a function of λ only in the present case. This function (divided by h), is depicted in Fig. 4. Eq. (3.39) is straightforward to integrate from the eastern boundary, along the rays, yielding

$$|\hat{p}_{\mathrm{s}}|^2(\lambda,\xi) = \underbrace{\frac{\chi(\lambda)h(\lambda_{\mathrm{E}})}{h(\lambda)}\frac{1+\alpha^2 S_n^2(\alpha)}{1-\alpha+\alpha^2 S_n^2(\alpha)}}_{G^2(\lambda)}|\hat{p}_{\mathrm{s}}|^2(\lambda_{\mathrm{E}},\xi), \tag{3.41}$$

where we assumed $\alpha(\lambda_{\mathrm{E}}) = 0$ along the eastern boundary. To obtain the expression for $|\hat{p}_{\mathrm{s}}|$ as a function of longitude and latitude, we invert the relation $\sin\phi = \chi(\lambda)\sin\xi$, which yields $\xi = \arcsin[\sin\phi/\chi(\lambda)]$, hence

$$|p_{\mathrm{s}}|(\lambda,\phi) = G(\lambda)|\hat{p}_{\mathrm{s}}|(\lambda_{\mathrm{E}},\arcsin[\sin\phi/\chi(\lambda)]). \tag{3.42}$$

The latitudinal variations of $|\hat{p}_{\mathrm{s}}|$ when topography varies with longitude only are therefore entirely linked to its latitudinal variations along the eastern boundary. If χ is close to unity, the last term does not differ much from $|\hat{p}_{\mathrm{s}}|(\lambda_{\mathrm{E}},\phi)$. The equation for the amplitude $|A|$ follows from that for $|\hat{p}_{\mathrm{s}}|$,

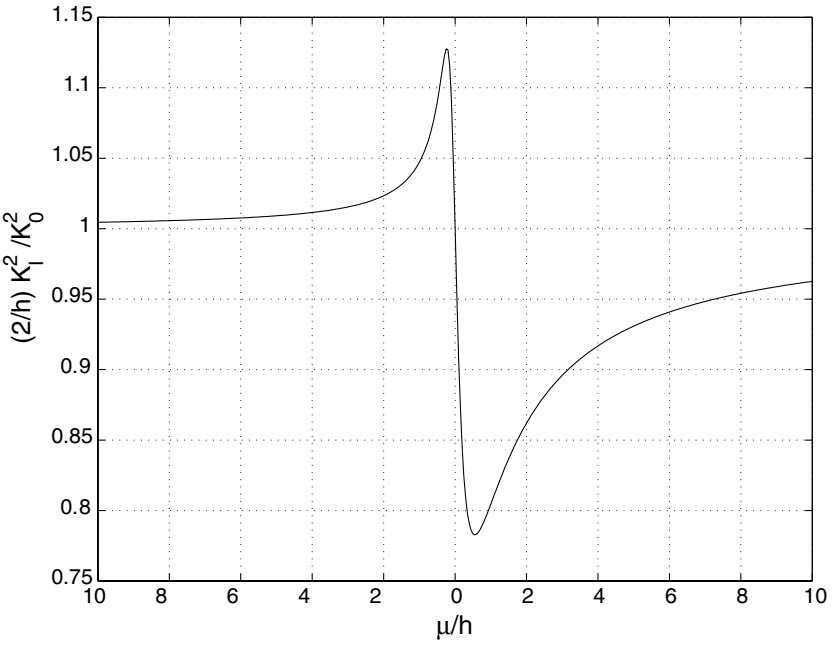

Fig. 4. The function $(2/h)K_{\mathrm{I}}^2/K_0^2$ of the parameter μ/h. This function partly controls the ratio of the squared SSH to its value along the eastern boundary (see Eqs. (3.40) and (3.41)).

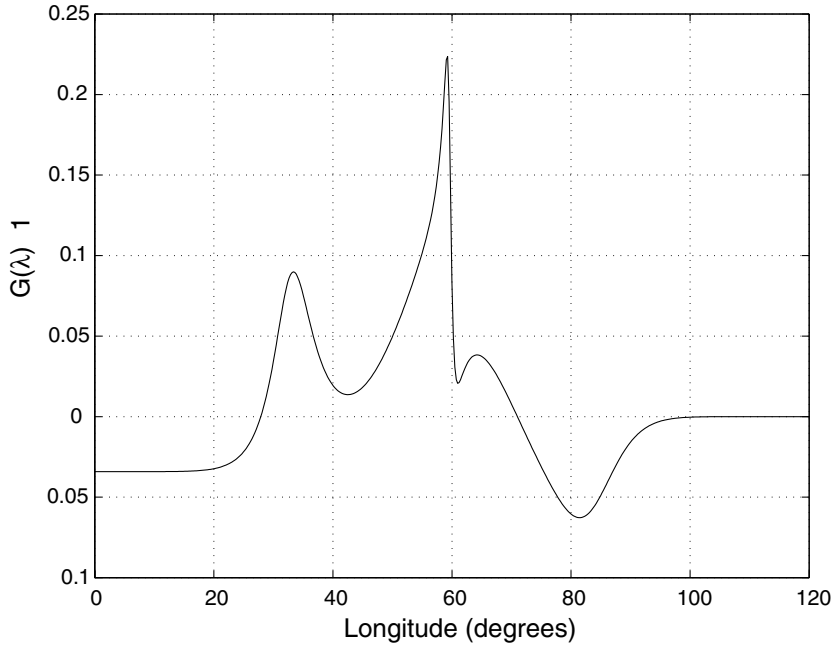

Fig. 5. The function $G(\lambda) - 1 = |p_s(\lambda, \xi)|/|p_s(\lambda_E, \xi)| - 1$ as a function of longitude.

$$|A|(\lambda, \xi) = |\hat{p}_s|/F'(0) = \gamma(\lambda)G(\lambda)|A|(\lambda_E, \xi), \tag{3.43}$$

using the result that $F'(0) = 1/\gamma$ from (3.11) (taking $F_0 = 1$.) Note that since we chose M_0 real, we have $A = |A|$ here. The departure of $G(\lambda)$ from unity is depicted in Fig. 5. We see that the surface height anomaly first decreases along the ridge's eastern flank, to then increases by about 20 percent near its top, after which it fluctuates on the western flank. In the western flat bottom part, the amplitude is about 4 percent less than it was initially along the eastern boundary. To be consistent with the WKB assumption, $G(\lambda)$ should vary over scales much larger than k_λ^{-1}. This is clearly not the case near the hilltop, which sees dramatic relative variations of G over much less than a wavelength. This is a visual indication that WKB must breakdown there. For this reason, the reader should be aware before to proceed to the next section that the WKB solution in the western part of the basin is bound to misrepresent some features of the actual solution. This point is further discussed in Section 5, and also in Tailleux and McWilliams (2002) in the two-layer model case.

4. Illustrations for the leading order wave mode

4.1. Depth/longitude sections of the modal structure

In this paragraph, we investigate the evolution of the vertical structure of the modes along the rays. This issue was recently studied in a two-layer QG model by Hallberg (1997), who found the

modes to undergo fast variations in localized regions where he argued should exist linear coupling between two different WKB modes. This was later interpreted by Vanneste (2001) within the framework of linear mode conversion theory. Interest in the vertical structure of the perturbations is also motivated by the possibility of using general circulation models, which in principle provide access to it, for testing the various Rossby waves theories currently under development, and to derive constraints on the interior dynamics from surface observations of the waves propagation. The behavior of $-M = -\gamma G \sin(\sigma/\gamma)$ and $\mathrm{d}M/\mathrm{d}\sigma = G(\lambda)\cos(\sigma/\gamma)$ is depicted in Fig. 6. The top panel represents the perturbation wave field associated with the buoyancy and vertical velocity,

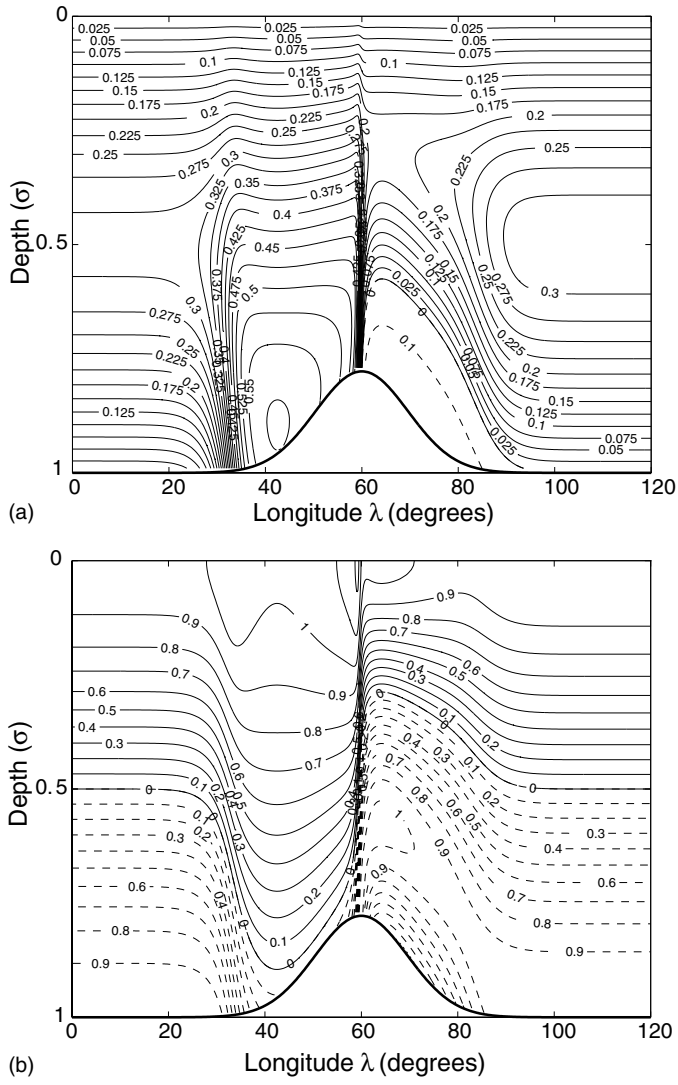

Fig. 6. Depth/longitude sections of the wave perturbations. (a) For the vertical velocity and buoyancy; (b) for the horizontal velocity and pressure.

while the bottom panel represents the perturbation wave field associated with the pressure, and horizontal velocity. In the flat western and eastern parts, the wave perturbation exhibits the classical standard first-mode baroclinic structure, characterized by a change of sign at mid depth for the pressure perturbation, and by a maximum for the vertical velocity. The most salient features are the increase in vertical complexity on the eastern flank, characteristic of a modal structure closer to that of a second mode, with a phase speed slower than standard. In contrast, the vertical structure appears equivalent barotropic on the western flank. Furthermore, we note that the pressure perturbation there vanishes near the bottom, and thus possesses a vertical modal structure close to that of the bottom pressure compensated modes studied in Tailleux and McWilliams (2001). These modes are always associated with a faster propagation than standard, which the latter study shows can be of the same order of magnitude as those observed by Chelton and Schlax (1996) when using realistic buoyancy frequency profiles. We note that the transition in vertical structure from the eastern to western flank occurs in a very confined region around the hilltop, and thus resembles the rapid transition behavior evidenced by Hallberg (1997). The visual impression is that of a quasi-discontinuous change. Less important, but nevertheless quite rapid is the transition from the flat-bottom regions to the ridge's flanks, especially in the western part. On the other hand, the transition taking place in the eastern part appears quite smooth.

The examination of the solution suggests to isolate three different transition regions, for which three different "critical" length scales L_w, L_t and L_e can be defined, associated respectively with the western, hilltop, and eastern transitions. The Fig. 6 shows that in the present example,

$$L_t < L_w < L_e. \tag{4.1}$$

In the present model, these length scales depend essentially upon the particular geometry considered, and not upon the wavelength of the waves studied. This is because they are related to the behaviour of the nonlinear ODE for Z, as well as upon the way the eigensolutions vary with the parameter μ and h, which do not depend explictly upon the wavenumbers. [3] Since L_t is the smallest of the above length scales, it is the one which defines the most stringent condition on the maximum wavelength admissible for WKB to remain accurate across the whole basin. In the present case, a zoom of Fig. 6 centered on the hilltop, depicted in Fig. 7, shows that L_t is about 1–1.5° wide, and hence $\mathcal{O}$ (50–150 km) depending on the latitude considered. Interestingly, we note that this fast transition region appears to be slightly off the hilltop on the western flank. This differs from the two-layer model case studied by Tailleux and McWilliams (2002) where the latter occurred also slightly off the hilltop, but on the eastern flank.

The above-defined critical length scales are not easily related to the parameters of the problem, as for instance the length scale λ_T entering the Gaussian topography (2.21). The problem is complicated by the fact that it depends on both the variations of the amplitude and that of the parameter $\mu = Zh'$, for which no analytical solution exists. Clearly, further work is needed to solve this issue. We postulate that the problem can be resolved by extending the results of mode conversion theory to the present case. Assuming this can be done, we would expect the critical length scales to be strongly controlled by the local curvature of the topography, provided that the

[3] The wavenumber independence of the vertical structure is potentially altered if dispersive effects are retained, because then the ray equations would depend on the wavenumbers.

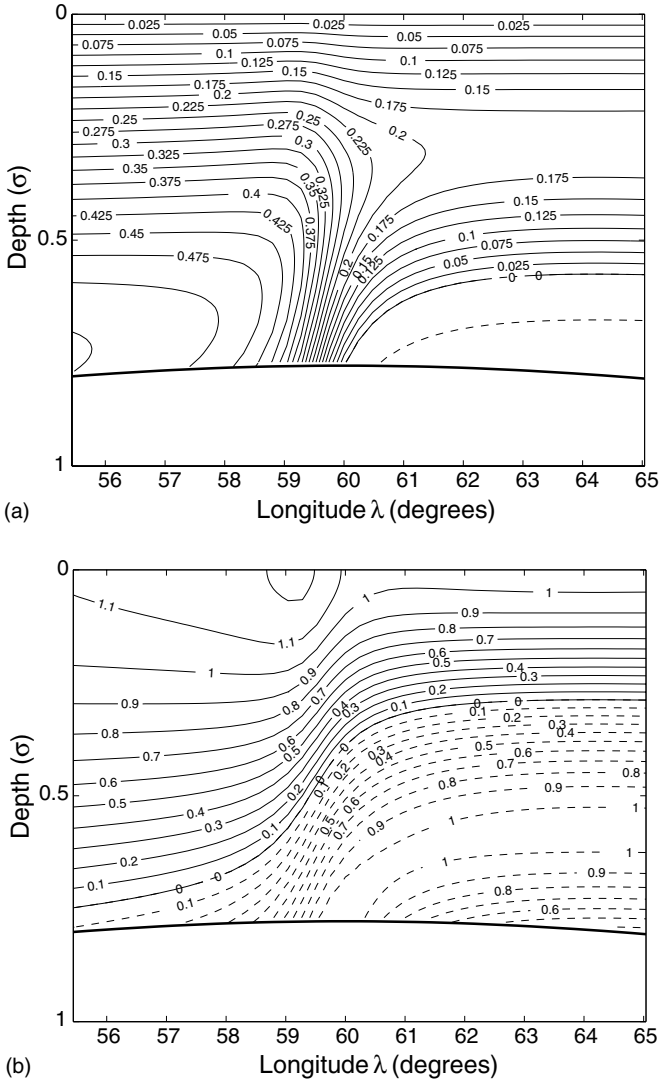

Fig. 7. Zoom of the previous figure centered on the basin center.

two-layer model results (e.g., Vanneste, 2001; Hallberg, 2001; Tailleux and McWilliams, 2002) are meaningful to interpret the continuously stratified case.

4.2. Hoevmuller diagrams

Another application of practical interest is the construction of longitude/time plots, also called Hoevmuller diagrams, of the surface pressure anomaly. These diagrams constitute indeed the simplest way to visualize the westward propagation of Rossby waves in the altimeter data. Such diagrams form also the basis for all empirical determinations of the Rossby wave propagation, by

means of the Radon transform for instance (e.g., Chelton and Schlax, 1996). Specifically, the quantity of interest is

$$p_s(\lambda,\phi,t) = A(\lambda)F'(0)\cos\left(\Sigma(\lambda,\phi) - \omega t\right) = G(\lambda)\cos(\Sigma(\lambda,\phi) - \omega t), \tag{4.2}$$

where

$$\Sigma - \omega t = \omega\left[\sin^2\phi\int_{\lambda}^{\lambda_E}\frac{\mathrm{d}\lambda'}{\Gamma(\lambda')}\,\mathrm{d}\lambda' - t\right]. \tag{4.3}$$

To plot (4.2) for a given latitude ϕ, we need the value of the dimensionless frequency ω. The latter is related to the dimensional frequency ω_0 by

$$\omega = \omega_0\frac{2\Omega R^2}{N_0^2 H_0^2}$$

(from (2.11)). Here, we used the values $N_0 = 5\times10^{-3}$ s^{-1}, $H_0 = 4500$ m, $\omega_0 = 2\pi/(1\text{ year})$, $\Omega = 2\pi/(1\text{ day})$, and $R = 6.4\times10^6$ m, yielding $\omega \approx 2.3430$. The expression (4.2) was plotted in Fig. 8 assuming G constant over longitude (top panel), as well as by accounting for its full variations (bottom panel), in order to assess the importance of the amplitude variations on the visual impression of westward propagation. The figure shows that in this particular example there is little difference between the two panels.

The visual impression of westward propagation is related to the slopes of the isolines for p_s. An expression for the latter is obtained by differentiating (4.2) for fixed ϕ, yielding

$$\frac{\mathrm{d}\lambda}{\mathrm{d}t} = -\frac{\omega}{k_\lambda}\frac{1}{1-\dfrac{G'(\lambda)}{k_\lambda G(\lambda)}\dfrac{\cos(\Sigma-\omega t)}{\sin(\Sigma-\omega t)}} = \frac{c_{p\lambda}}{1-\kappa(\lambda,\phi,t)} = -\frac{\Gamma}{\sin^2\phi}\frac{1}{1-\kappa}. \tag{4.4}$$

The little differences between the two panels of Fig. 8 indicate that the coefficient κ entering Eq. (4.4) has little impact on the visual impression of westward propagation. As a result, we expect the slopes $\mathrm{d}\lambda/\mathrm{d}t$ for the isolines of p_s to be essentially governed by $c_{p\lambda}$, and hence by $\Gamma(\lambda)$ for fixed ϕ. This provides evidence that the zonal phase speed $c_{p\lambda} = \omega/k_\lambda$, not the zonal group velocity $c_{g\lambda}$, is the relevant quantity to interpret the results of Chelton and Schlax (1996). This by itself is worthy of note, because although several authors have advocated for the use of $c_{p\lambda}$, evidence that the amplitude variations has no influence on the apparent phase speeds has been lacking so far.

5. A posteriori estimate of the approximation residual

The previous diagnostics provides empirical evidence for the existence of critical length scales defining the upper admissible wavelength above which WKB breakdown becomes inevitable. We can get further insight into this issue by looking into what controls the next-order correction term, which is solution of the following problem:

$$-\mathrm{i}\omega\frac{\mathrm{d}^2M_1}{\mathrm{d}\sigma^2} + \frac{v^2\mathrm{i}k_\lambda}{\sin^2\phi}M_1 = \mathscr{R}_0 \Longleftrightarrow -\mathrm{i}\omega\left[\frac{\mathrm{d}^2M_1}{\mathrm{d}\sigma^2} + \frac{v^2}{\gamma^2}M_1\right] = \mathscr{R}_0, \tag{5.1}$$

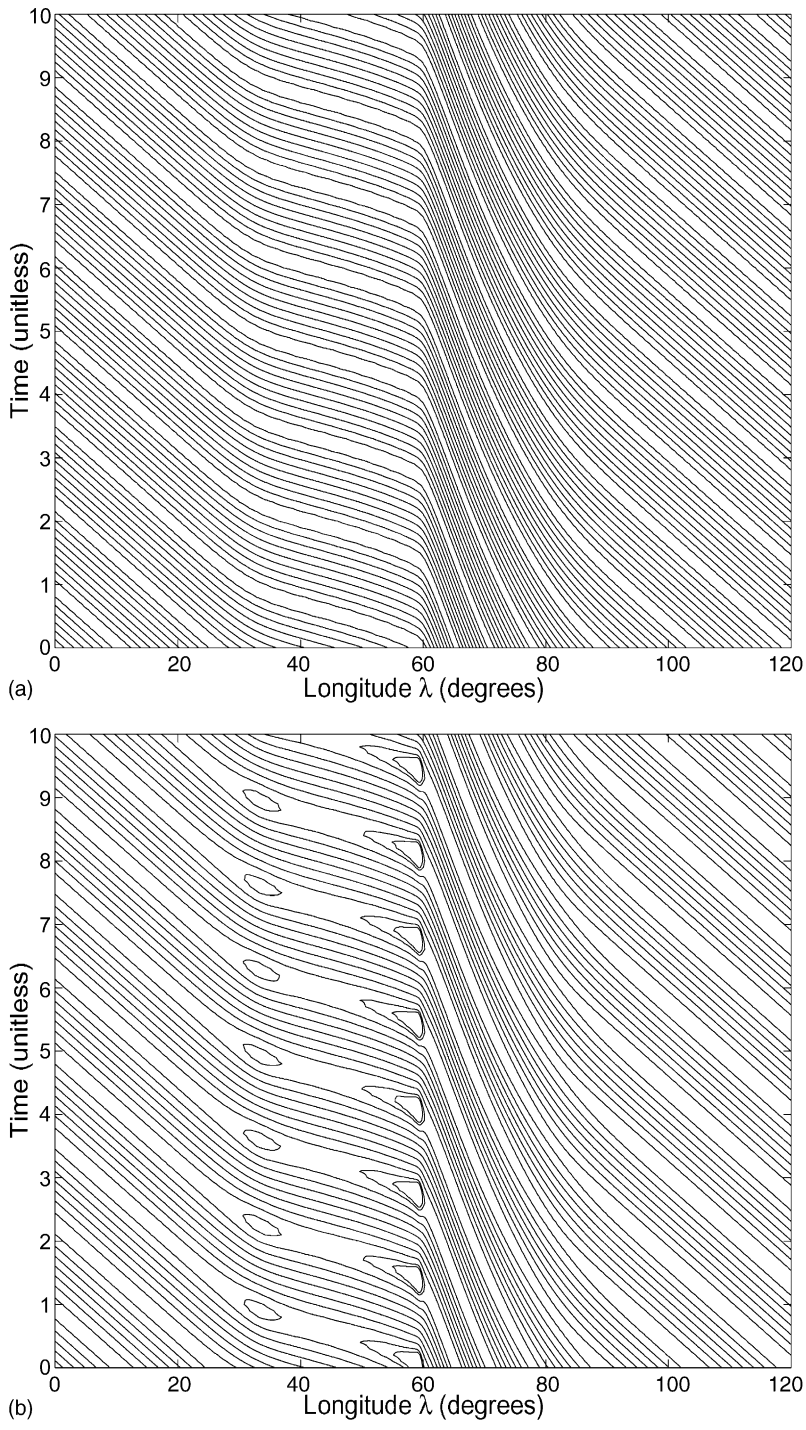

Fig. 8. Longitude/time plots for the surface pressure perturbations at the latitude 45°. (a) Assuming $G(\lambda) = G(\lambda_E) = cst$; (b) Taking into account the longitudinal variations of $G(\lambda)$.

$$M_1(0) = 0, \tag{5.2}$$

$$\mathrm{i}k_\lambda\left[M_1(-h) - \mu M_1'(-h)\right] = \mathscr{B}_0, \tag{5.3}$$

where

$$\mathscr{R}_0 = -\frac{v^2}{\sin^2\phi}\frac{\partial M_0}{\partial\lambda}, \tag{5.4}$$

$$\mathscr{B}_0 = -\frac{\partial M_0}{\partial\lambda}(-h) + \tan\phi\left[\frac{\partial^2 M_0}{\partial\phi\,\partial\sigma}(-h)\frac{\partial h}{\partial\lambda} - \frac{\partial^2 M_0}{\partial\lambda\,\partial\sigma}(-h)\frac{\partial h}{\partial\phi}\right]. \tag{5.5}$$

In the constant buoyancy case, we have $M_0 = AF = A\sin(\sigma/\gamma)$, which yields

$$\mathscr{R}_0 = -\frac{1}{\sin^2\phi}\left[\frac{\partial A}{\partial\lambda}\sin(\sigma/\gamma) - \frac{A}{\gamma^2}\frac{\partial\gamma}{\partial\lambda}\sigma\cos(\sigma/\gamma)\right]. \tag{5.6}$$

With $v = 1$, and $\mathscr{R}_0$ given by (5.6), it is straightforward to express the general solution of (5.1) in the following analytical form:

$$M_1 = \frac{\mathrm{i}}{\omega\sin^2\phi}\left[\left(\frac{A}{4}\frac{\partial\gamma}{\partial\lambda} + \frac{\gamma}{2}\frac{\partial A}{\partial\lambda}\right)\sigma\cos(\sigma/\gamma) + \frac{A}{4\gamma}\frac{\partial\gamma}{\partial\lambda}\sigma^2\sin(\sigma/\gamma)\right] + C_2\sin(\sigma/\gamma), \tag{5.7}$$

or equivalently, using the dispersion relation (3.15),

$$M_1 = -\frac{\mathrm{i}}{\Gamma k_\lambda}\left[\left(\frac{A}{4}\frac{\partial\gamma}{\partial\lambda} + \frac{\gamma}{2}\frac{\partial A}{\partial\lambda}\right)\sigma\cos(\sigma/\gamma) + \frac{A}{4\gamma}\frac{\partial\gamma}{\partial\lambda}\sigma^2\sin(\sigma/\gamma)\right] + C_2\sin(\sigma/\gamma), \tag{5.8}$$

where C_2 is constant which can only be determined from the consideration of the next-order problem for M_2. This is not done here, both because this is tedious and not needed to get a first look at the validity of the leading order WKB approximation. As said previously, we can assume M_0, and hence A, purely real, in which case M_1 is purely imaginary. The consequence is to induce phase corrections. From the structure of M_1, we can identify two kind of phase corrections. The first one is related to the term proportional to C_2; it introduces at leading order a a phase correction $|\Delta\Sigma| \approx |C_2/A|$ (provided that $C_2 \ll A$) which depends only on the horizontal coordinates. The remaining part of M_1, however, induces a phase correction that also depends upon depth.

The solution (5.7) satisfies automatically (5.1), as well as the upper boundary condition (5.2). That it satisfies the bottom boundary condition (5.3) is more difficult to check directly, but is guaranteed from the way A was constructed (i.e., as the solvability condition for precisely (3.4)–(3.6)). Eq. (5.8) makes it clear that the correction term is inversely proportional to the zonal wavenumber. It follows that we can in principle make the leading order WKB approximation as accurate as we want by increasing k_λ, or equivalently by considering smaller and smaller wavelength. This is expected because acting on the wavelength is equivalent to acting on the WKB parameter ε. [4] The breakdown of the leading order WKB solution is thus dependent upon the particular values of the parameters considered. As an illustration, the vertical structure of $-\mathrm{i}M_1$ is depicted in Fig. 9, setting $C_2 = 0$ in (5.7), for the present case. The most interesting feature of the

[4] Note that for a given configuration where the buoyancy frequency and topography are externally imposed, the only way to decrease the wavelength is by increasing the frequency.

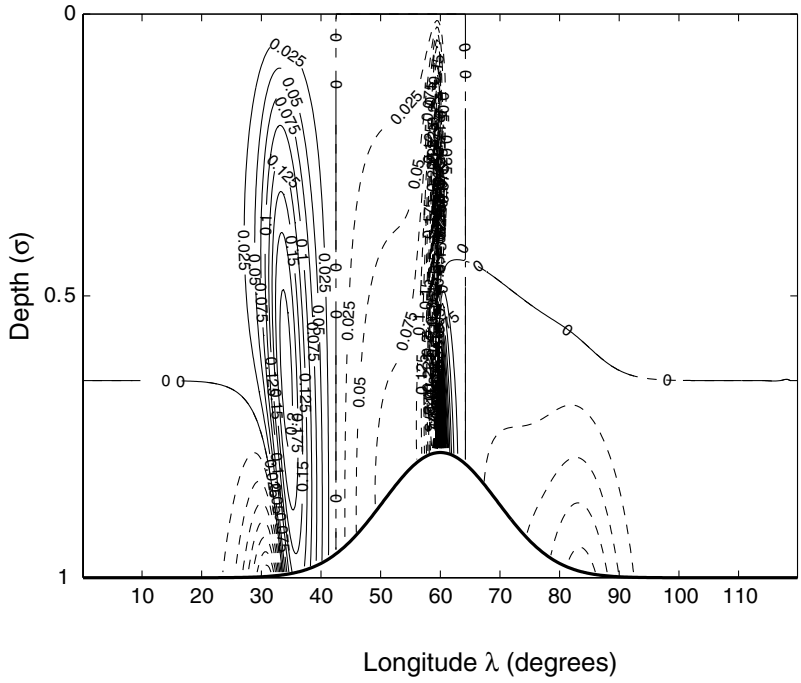

Fig. 9. Vertical/longitude section of the next-order correction term for the buoyancy/vertical velocity perturbation at $\phi = 45°$.

correction term is its structure, which unlike its amplitude is independent of the wavelength considered. We thus note that the correction term is very large in a confined region over the hilltop, quite large over a broader region on the western flank, and relatively small on the eastern flank. The structure of the correction term is therefore consistent with the ordering induced by the critical length scales defined previously. With the particular numerical values considered for this example, the leading order WKB approximation breaks down near the hilltop and on the western flank, for the amplitude of the correction term becomes of the same order of magnitude or higher than the leading order term there. By comparison, the WKB breakdown studied in Tailleux and McWilliams (2002) occurred on the hilltop and eastern flank. To obtain a valid leading order WKB approximation with the same stratification and topography would require considering considerably higher frequencies for which the use of PG equations would become problematic.

6. Discussion

This paper complemented previous WKB studies on the altered dynamics of baroclinic Rossby waves in presence of medium variations (here restricted to that of the topography only) by focusing on three distinct topics that have received little or no attention so far, for which the main results are:

- The waves' vertical structure is unambiguously linked to their phase speed. Specifically, faster propagation than standard is associated with an equivalent barotropic vertical structure that is close to that of the surface intensified modes that is the focus of TM01, while slower propagation is associated with an increase in vertical complexity that is intermediate between that of the first and second standard baroclinic modes. To go farther, it would be of interest to determine whether such a characterization can also be made when the effects of the background mean flow are retained. These results may provide a way to verify Rossby wave theories by means of ocean general circulation models, as the information on both the surface and vertical structure is readily available (although this may require some work to isolate the Rossby wave signal unambiguously).
- The visual impression of westward propagation in longitude/time sections of the sea surface height anomalies is dominated in the present solution by the phase variations, even though the amplitude does not necessarily vary smoothly everywhere. This supports the use the zonal phase speed ω/k_x as the quantity to be compared with the propagation speeds measured by Chelton and Schlax (1996), which have been advocated by a number of authors, but without a clear indication that amplitude variations could be safely neglected;
- The residual of the solution, as estimated by the computation of the next-order term of the formal WKB series expansion, is found to have a structure that varies strongly with longitude. Furthermore, it is found empirically to reach local extrema in three particular transition regions which coincide with the regions where the leading order approximation vary the most rapidly over three distinct critical length scales L_w, L_t, and L_e, corresponding respectively to the bottom western flank, hilltop, and eastern bottom flank regions. Because of the existence of these three length scales, the classical leading order WKB approximation can only be uniformly valid for wavelengths smaller than the smallest of these critical length scales, i.e., L_t in the present case. Since L_t is approximately of the order of 2° of longitude here, i.e., less than 200 km, this restricts the study to wavelengths that are close to that of the Rossby radius of deformation, which cannot be done without also rising concerns about the validity of using the PG equations. These length scales are not easily related to the length scales of the problem, so that further work is therefore needed to understand what determines their particular values. The empirical evidence for localized regions where the leading order WKB approximation varies the most rapidly is similar to the behaviour discussed by H97, and predicted by mode conversion theory. For this reason, it is tempting to speculate that the transition regions discussed here should correspond to the places of occurrence of mode conversion points. Furthermore, we also speculate that the above critical length scales are the quantity L_c actually predicted by mode conversion theory when writing the transmission coefficient under the form $T = e^{-k_\lambda L_c}$, where k_λ is the zonal wavenumber of the Rossby wave (e.g., see TM02). To verify this, the results of mode conversion theory need to be extended to the continuously stratified setting, which we hope to report on later.

Acknowledgements

Jacques Vanneste is gratefully acknowledged for comments and bringing to my attention the concept of the slowness vector. The comments of two anonymous reviewers greatly contributed to improve and clarify the manuscript.

Appendix A. Derivation of the K-coefficients for $\gamma^2 > 0$

We seek analytical expressions for the coefficients K_r^2, K_b^2, K_0^2 and K_I^2 which enter the ray equations in various places. Given that $F = F_0 \sin(\sigma/\gamma)$, we successively derive

$$F_b'^2 = \frac{F_0^2}{\gamma^2}\cos^2(h/\gamma) = \frac{F_0^2}{\gamma^2}\frac{1}{1+\tan^2(h/\gamma)} = \frac{F_0^2}{\gamma^2+\mu^2},$$

$$F_0'^2 = \frac{F_0^2}{\gamma^2},$$

$$\int_{-h}^{0} v^2F^2\,\mathrm{d}\sigma = F_0^2\int_{-h}^{0}\sin^2(\sigma/\gamma)\,\mathrm{d}\sigma = F_0^2\int_{-h}^{0}\frac{1-\cos(2\sigma/\gamma)}{2}\,\mathrm{d}\sigma,$$

$$= F_0^2\left(\frac{h}{2} - \left[\gamma\frac{\sin(2\sigma/\gamma)}{4}\right]_{-h}^{0}\right) = \frac{F_0^2}{4}(2h - \gamma\sin(2h/\gamma)) = \frac{F_0^2}{2}\left(h + \frac{\mu}{1+\mu^2/\gamma^2}\right),$$

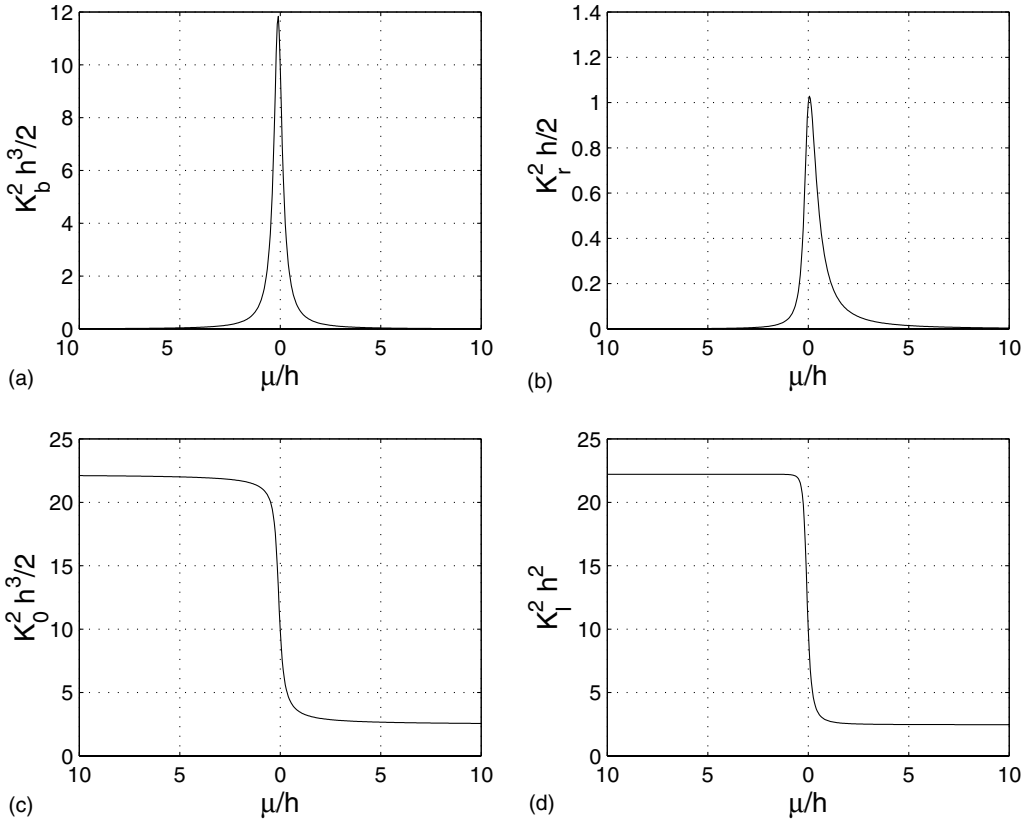

Fig. 10. The coefficients K_b^2 (a), K_r^2 (b), K_o^2 (c), and K_I^2 (d), normalized by some power of h to make them function of $\alpha = \mu/h$ only.

$$\int_{-h}^{0} F'^2\,\mathrm{d}\sigma = \frac{F_0^2}{\gamma^2}\int_{-h}^{0}\cos^2(\sigma/\gamma)\,\mathrm{d}\sigma = \frac{F_0^2}{2\gamma^2}\int_{-h}^{0}(1+\cos(2\sigma/\gamma))\,\mathrm{d}\sigma = \frac{F_0^2}{2\gamma^2}\left(h - \frac{\mu}{1+\mu^2/\gamma^2}\right).$$

To obtain the above expressions, we used the fact that $\tan(\mu/h) = -\mu/\gamma$ from (3.12) (restricting here to the case $\gamma^2 > 0$), and the classical expressions linking $\cos(2u)$ and $\sin(2u)$ to $\tan u$ for any argument u. From the above derivations, it is straightforward to establish the following expressions (using $\alpha = \mu/h$):

$$K_{\mathrm{b}}^2 = \frac{F_{\mathrm{b}}'^2}{\int_{-h}^{0} v^2F^2\,\mathrm{d}\sigma} = \frac{2}{\gamma^2}\frac{1}{h(1+\mu^2/\gamma^2)+\mu} \Rightarrow \frac{h^3K_{\mathrm{b}}^2}{2} = \frac{S_n^2(\alpha)}{1+\alpha+\alpha^2S_n^2(\alpha)},$$

$$K_{\mathrm{I}}^2 = \frac{\int_{-h}^{0} F'^2\,\mathrm{d}\sigma}{\int_{-h}^{0} v^2F^2\,\mathrm{d}\sigma} = \frac{1}{\gamma^2}\frac{h(1+\mu^2/\gamma^2)-\mu}{h(1+\mu^2/\gamma^2)+\mu} \Rightarrow h^2K_{\mathrm{I}}^2 = S_n^2(\alpha)\frac{1-\alpha+\alpha^2S_n^2(\alpha)}{1+\alpha+\alpha^2S_n^2(\alpha)},$$

$$K_0^2 = \frac{F_0'^2}{\int_{-h}^{0} v^2F^2\,\mathrm{d}\sigma} = \frac{2}{\gamma^2}\frac{1+\mu^2/\gamma^2}{h(1+\mu^2/\gamma^2)+\mu} \Rightarrow \frac{h^3K_0^2}{2} = S_n^2(\alpha)\frac{1+\alpha^2S_n^2(\alpha)}{1+\alpha+\alpha^2S_n^2(\alpha)},$$

$$K_{\mathrm{r}}^2 = \frac{K_{\mathrm{b}}^2}{K_{\mathrm{I}}^2} = \frac{F_{\mathrm{b}}'^2}{\int_{-h}^{0} F'^2\,\mathrm{d}\sigma} = \frac{2}{h(1+\mu^2/\gamma^2)-\mu} \Rightarrow \frac{hK_{\mathrm{r}}^2}{2} = \frac{1}{1-\alpha+\alpha^2S_n^2(\alpha)}.$$

This shows that all the coefficients, as well as the gravity wave speed, are all separable function of h and $\alpha = \mu/h$. These four coefficients are displayed in Fig. 10.

References

Allen, J.S., Romea, R.D., 1980. On coastal trapped waves at low latitudes in a stratified ocean. J. Fluid Mech. 98, 555–585.

Bender, C.M., Orszag, S.A., 1978. Advanced mathematical methods for scientists and engineers. Springer., 593 pp.

Bobrovich, A.V., Reznik, G.M., 1999. Planetary waves in a stratified ocean of variable depth. Part2. Continuously stratified ocean. J. Fluid Mech. 388, 147–169.

Cessi, P., Paparella, F., 2001. Excitation of basin modes by ocean–atmosphere coupling. Geophysical Research Letters 28, 2437–2440.

Chelton, D.B., Schlax, M.G., 1996. Global observations of oceanic Rossby waves. Science 272, 234–238.

Colin de Verdière, A., 1988. Buoyancy-driven planetary flows. J. Mar. Res. 46, 215–265.

de Szoeke, R.A., Chelton, D.B., 1999. The enhancement of planetary wave speeds by homogeneous potential vorticity layers. J. Phys. Oceanogr. 29, 500–511.

Dewar, W.K., 1998. On ''too fast'' baroclinic planetary waves in the general circulation. J. Phys. Oceanogr. 28, 1739–1758.

Dickinson, R.E., 1978. Rossby waves—Long-period oscillations of oceans and atmospheres. Ann. Rev. Fluid Mech. 10, 159–195.

Flynn, W.G., Littlejohn, R.G., 1994. Normal forms for linear mode conversion and Landau–Zener transitions in one dimension. Ann. Phys. 234, 334–403.

Gallego, B., Cessi, P., 2000. Exchange of heat and momentum between the atmosphere and the ocean: a minimal model of decadal oscillations. Journal of Climate 16, 479–489.

Gill, A.E., 1982. Atmosphere–Ocean Dynamics. Academic Press., 662 pp.

Gorman, A.D., Yang, H.J., 2001. Caustic consideration of long planetary wave packet analysis in the continuously stratified ocean. Int. J. Math. Math. Sci. 25, 63–71.

Grimshaw, R., Allen, J.S., 1979. Linearly coupled, slowly varying oscillators. Studies Appl. Math. 61, 55–71.

Hallberg, R., 1997. Localized coupling between surface and bottom-intensified flow over topography. J. Phys. Oceanogr. 27, 977–998.
Hallberg, R., 2001. Reply to (Comments on localized coupling between surface and bottom intensified flow over topography). J. Phys. Oceanogr. 31, 1926–1930.
Holland, W.R., 1967. On the wind-driven circulation in an ocean with bottom topography. Tellus 19, 582–599.
Kaufman, A.N., Friedland, L., 1987. Phase-space solution of the linear mode conversion problem. Phys. Lett. A 123, 387–389.
Kaufman, A.N., Morehead, J.J., Brizard, A.J., Tracy, E.R., 1999. Mode conversion in the Gulf of Guinea. J. Fluid Mech. 394, 175–192.
Killworth, P.D., Blundell, J., 1999. The effect of bottom topography on the speed of long extratropical planetary waves. J. Phys. Oceanogr. 29, 2689–2710.
Killworth, P.D., Blundell, J., 2001. Large-scale propagating disturbances: approximation by vertical normal modes. J. Phys. Oceanogr. 31, 2852–2870.
Killworth, P.D., Blundell, J., 2002a. Long extra-tropical planetary wave propagation in the presence of slowly varying mean flow and bottom topography. I: The local problem. J. Phys. Oceanogr., in press.
Killworth, P.D., Blundell, J., 2002b. Long extra-tropical planetary wave propagation in the presence of slowly varying mean flow and bottom topography. II: Ray propagation and comparison with observations. J. Phys. Oceanogr., in press.
Killworth, P.D., Chelton, D.B., deSzoeke, R., 1997. The speed of observed and theoretical long extratropical planetary waves. J. Phys. Oceanogr. 27, 1946–1966.
Leblond, P., Mysak, 1978. Waves in the Ocean. Elsevier., 602 pp.
Lighthill, J., 1978. Waves in Fluids. Cambridge University Press., 504 pp.
Liu, Z.Y., 1999. Planetary waves in the thermocline: non-doppler-shift mode, advective mode and green mode. Quart. J. Roy. Meteor. Soc. 125, 1315–1339.
Lorenz, E.N., 1955. Available potential energy and the maintenance of the general circulation. Tellus 7, 157–167.
Pedlosky, J., 1987. Geophysical Fluid Dynamics. Springer.
Polito, P.S., Cornillon, P., 1997. Long baroclinic Rossby waves detected by TOPEX/Poseidon. J. Geophys. Res. Oceans 102, 3215–3235.
Reznik, G.M., Tsybaneva, T.B., 1999. Planetary waves in a stratified ocean of variable depth. Part 1. Two-layer model. J. Fluid Mech. 388, 115–145.
Rhines, P.B., 1970. Edge-, bottom-, and Rossby waves in a rotating stratified fluid. Geophys. Fluid Dyn. 1, 273–302.
Rhines, P.B., Bretherton, F., 1973. Topographic Rossby waves in a rough-bottomed ocean. J. Fluid. Mech. 61, 583–607.
Samelson, R.M., 1992. Surface-intensified Rossby waves over rough topography. J. Mar. Res. 50, 367–384.
Shepherd, T.G., 1990. Symmetries, conservation laws, and Hamiltonian structure in geophysical fluid dynamics. Adv. Geophys. 32, 287–338.
Shepherd, T.G., 1993. A unified theory of available potential energy. Atmos. Ocean XXXI, 1–26.
Sirven, J., Frankignoul, C., 2000. Variability of the thermocline due to a sudden change in the Ekman pumping. J. Phys. Oceanogr. 30, 1776–1789.
Straub, D.N., 1994. Dispersion of Rossby waves in the presence of zonally varying topography. Geophys. Astrophys. Fluid Dyn. 75, 107–130.
Tailleux, R., 2002a. On the ray dynamics of long baroclinic Rossby waves over topography. J. Phys. Oceanogr., submitted for publication.
Tailleux, R., 2002b. Comments on the effect of bottom topography on the speed of long extratropical planetary waves. J. Phys. Oceanogr., submitted for publication.
Tailleux, R., McWilliams, J.C., 2000. Acceleration, creation, and depletion of wind-driven, baroclinic Rossby waves over an ocean ridge. J. Phys. Oceanogr. 30, 2186–2213.
Tailleux, R., McWilliams, J.C., 2001. The effect of bottom pressure decoupling on the speed of extratropical, baroclinic Rossby waves. J. Phys. Oceanogr. 31, 1461–1476.
Tailleux, R., McWilliams, J.C., 2002. On the propagation of energy of long extratropical Rossby waves over slowly-varying topography. J. Fluid Mec. 473, 295–319.

Vanneste, J., Shepherd, T.G., 1999. On wave action and phase in the non-canonical Hamiltonian formulation. Proc. R. Soc. Lond. A 455, 3–21.

Vanneste, J., 2001. Mode conversion for Rossby waves over topography: Comments on Localized coupling between surface and bottom-intensified flow over topography. J. Phys. Oceanogr. 31, 1922–1925.

Vanneste, J., 2003. Nonlinear dynamics over rough topography: barotropic and stratified quasi-geostrophic theory. J. Fluid Mech. 474, 299–318.

Welander, P., 1959. An advective model of the ocean thermocline. Tellus 11, 309–318.

Yang, H.J., 2000. Evolution of long planetary wave packets in a continuously stratified ocean. J. Phys. Oceanogr. 30, 2111–2123.